Central antarctic climate response to the solar cycle

D. M. Volobuev

Climate Dynamics
Observational, Theoretical and Computational Research on the Climate System

ISSN 0930-7575

Clim Dyn
DOI 10.1007/s00382-013-1925-3

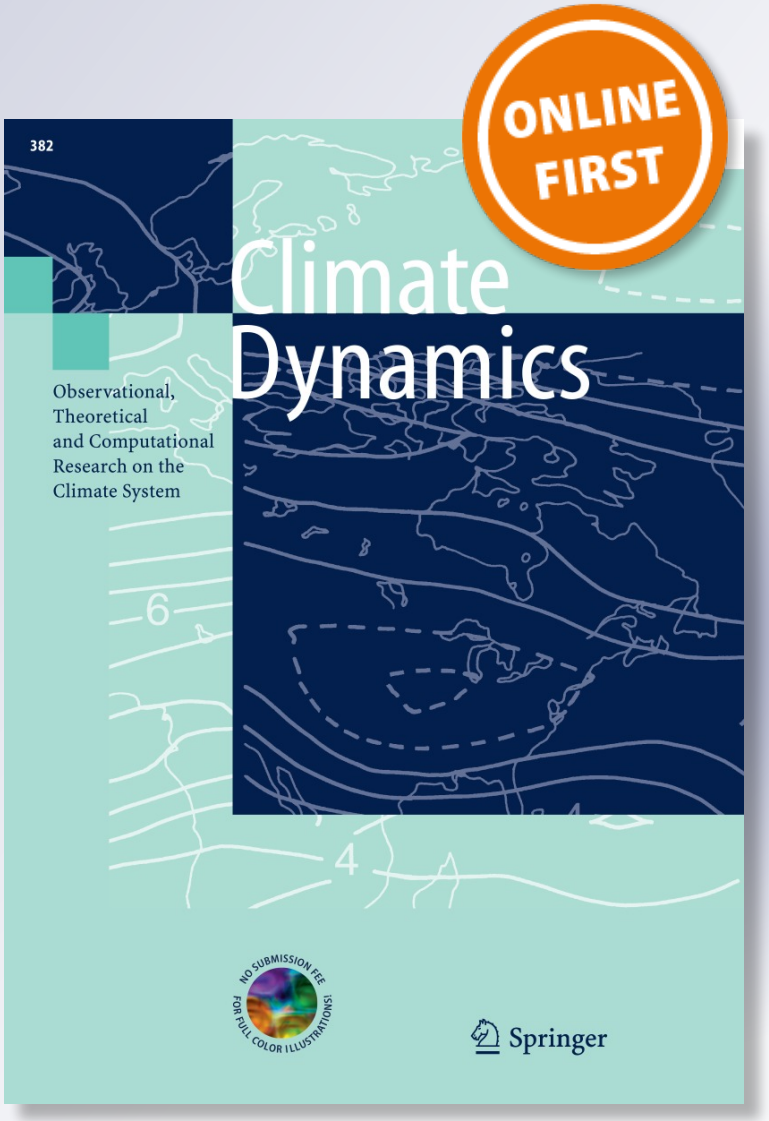

Springer

Clim Dyn
DOI 10.1007/s00382-013-1925-3

Central antarctic climate response to the solar cycle

D. M. Volobuev

Received: 26 December 2012 / Accepted: 19 August 2013

Abstract Antarctic "Vostok" station works most closely to the center of the ice cap among permanent year-around stations. Climate conditions are exclusively stable: low precipitation level, cloudiness and wind velocity. These conditions can be considered as an ideal model laboratory to study the surface temperature response on solar irradiance variability during 11-year cycle of solar activity. Here we solve an inverse heat conductivity problem: calculate the boundary heat flux density (HFD) from known evolution of temperature. Using meteorological temperature record during (1958–2011) we calculated the HFD variation about 0.2–0.3 W/m^2 in phase with solar activity cycle. This HFD variation is derived from 0.5 to 1 °C temperature variation and shows relatively high climate sensitivity per 0.1 % of solar radiation change. This effect can be due to the polar amplification phenomenon, which predicts a similar response 0.3–0.8 °C/0.1 % (Gal-Chen and Schneider in Tellus 28:108–121, 1975). The solar forcing (TSI) is disturbed by volcanic forcing (VF), so that their linear combination TSI + 0.5VF empirically provides higher correlation with HFD ($r = 0.63 \pm 0.22$) than TSI ($r = 0.50 \pm 0.24$) and VF ($r = 0.41 \pm 0.25$) separately. TSI shows higher wavelet coherence and phase agreement with HFD than VF.

Keywords Solar cycle · Antarctic climate · IHCP

D. M. Volobuev (✉)
Pulkovo Observatory, 196140, Pulkovskoe sh. 65/1,
Saint Petersburg, Russia
e-mail: dmitry.volobuev@mail.ru

1 Introduction

It is now well confirmed with satellite observations that solar luminosity changes by about 0.1 % during the 11-year solar cycle (Wilson and Mordvinor 2003; Frolich and Lean 1998; Foukal et al. 2006). This value is too small to see its direct influence on the earth surface temperature, but modeling and statistical tools can help (e.g. Stevens and North 1996; Scafetta and West 2007; Zhou and Tung 2010). It was estimated by Budyko (1968) that global climate sensitivity is 1 °C per 1 % of solar radiation change. This global estimation was confirmed by later studies, e.g. Gregory et al. 2004; Kiehl 2007; Gregory and Forster 2008 but remains highly uncertain (Schwartz 2007; Knutti et al. 2008). Major uncertainty is the heat capacity of the climate system that lags its response to forcings. This lag is often seen in reported local correlations (e.g. Eichler et al. 2009; Sirocko et al. 2012) but this lag is typically difficult to explain due to high-amplitude random forcings. Any observational constrain would be helpful in this case and we hope to estimate one of them. Local climate sensitivity varies considerably if response to 11-year solar cycle is considered (Stevens and North 1996). Dynamical feedback may increase climate sensitivity to luminosity or other forcing at polar regions by a few times (Gal-Chen and Schneider 1975; Langen and Alexeev 2007) not only due to surface albedo change with latitude but also due to increased longwave forcing on the high-latitude surface temperature (Schneider et al. 1999).

Among periods of luminosity oscillation, one-year seasonal and 11-year Schwabe cycles are strongest and most studied. Longer periods are questionable, although there are some reasons to believe them. Several reconstructions of solar irradiance were published (Lean et al. 1995; Solanki and Fligge 1999) based on the correlations

Published online: 03 September 2013

between solar activity and solar irradiance, but these correlations are established for relatively short period of solar irradiance observations with satellite based radiometers. Long-term trends of solar irradiance are subjects for scientific debates (Foukal et al. 2006) and we should conclude that there is no experimental evidence for these trends. In this work we will use one of most advanced reconstructions of TSI by Wang et al. (2005) for the evaluation of most pronounced 11-year solar cycle. Short-term seasonal cycle is very strong but is not global because it changes mostly the balance of incoming solar radiation between hemispheres whereas smaller global irradiation variations are difficult to reveal. In scope of climate science 11-year Schwabe cycle forcing is probably most important.

Here we analyze long enough (almost five solar cycles) meteorological temperature record near the center of Antarctic plateau as available at Vostok station (78°27′S 106°52′E). Regular meteorological conditions with almost zero low cloudiness and weak winds allow us to consider Vostok station as one of the best places on the Earth for solving the climate modeling problems.

Details on data analysis and preprocessing are shown in Sect. 2. An inverse problem is solved to estimate the heat flux density (HFD) variation on the ice surface from given temperature near the surface (Sect. 3). Results are discussed in Sect. 4.

2 Data

Regular observations on Vostok start in 1958 and meteodata are available since this time. During four winters (1962, 1994, 1996, 2003 years) the station was closed due to logistic problems, and several monthly gaps are present in observations. We estimated annual mean surface air temperature on the base of these data. If number of gaps were <2 during a year, monthly gaps were filled with linear interpolation between the same months in adjacent years. If three or more months during the year were lost, we used the smoothing spline to fill the gap in yearly means. Smoothing spline is a commonly used algorithm of data approximation with a cubic spline minimizing the weighted sum

$$p\sum (y_i - S_i)^2 + (1-p)\int (D^2 S(t))^2 dt$$

of errors between spline (S) and data (y) and the norm of the second derivative of the spline ($D^2S(t)$) in a functional form, p is a smoothing parameter. We use $p = 1/(1 + h^3/a)$, there sampling rate h = 1 year, parameter a = 0.5 is appropriately chosen, smaller parameter leads to smoother curve (Fig. 1). Smoothing spline algorithm can be found in Fortran subroutine CUBSPL or MatLab Spline Toolbox

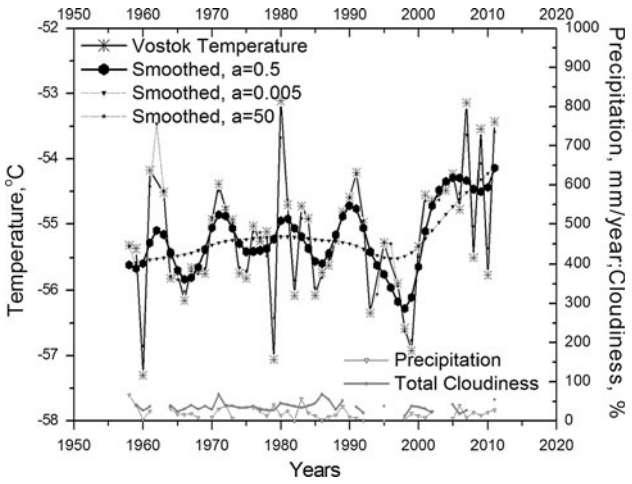

Fig. 1 Vostok annual surface air temperature and its smoothing spline (*left axis*), precipitation and total cloudiness index (*right axis*)

function CSAPS. Although ground surface temperatures are also available at Vostok we avoid using them as the model input due to two reasons (1) this data have more gaps and (2) they have good correlation and correct negative deviation respective to surface air temperature during first 20 years only. During more recent period ground temperature rises higher than air temperature and correlation becomes smaller. Higher ground temperature is inconsistent with global heat balance of polar regions theory and observations (Chen et al. 2010). This higher ground temperature effect is likely due to local heat pollution of the ground originated from year-around heating of the radiohome which is spaced some tenths of meters from the spot with meteorological instruments. The home was suspended on the piles during first years after the station was built and this essentially prevents the ground from the heat pollution. Drifting snow during the years filled the gap between the home and the ground so that the home was essentially covered with the snow during recent decades and heat may sink into ice. So we expect that surface air temperature is more accurate during all the period of observations.

Initial data for monthly surface air temperatures are available at http://www.aari.aq/data/data.asp?lang=0&station=6 (courtesy of AARI and RAE team).

The smoothing spline simulteneously smoothes the data and provides the possibility for accurate estimation of the first differenses from the smoothed data in functional form. Initial and smoothed temperature data are presented in Fig. 1 with time series for precipitation and total cloudiness for better understanding of local meteorological conditions. Wind velocities are available during recent 7 years with total average 4.6 m/s. Cloudiness, precipitation and wind velocities are smaller than average during the Antarctic summer. Low level cloudiness is close to zero, so presented total cloudiness is mostly high level cloudiness as

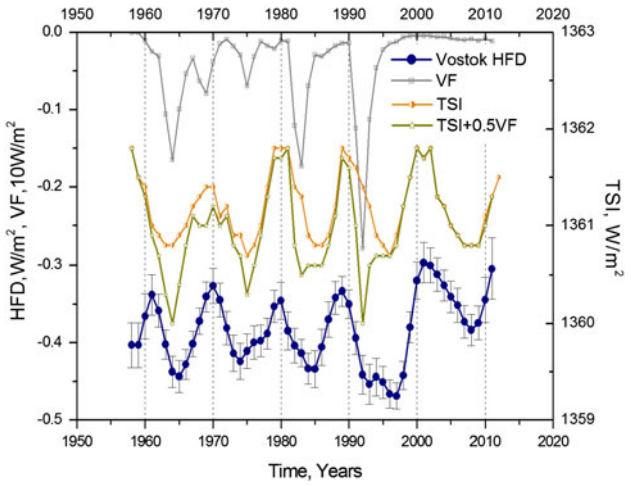

Fig. 2 Heat flux density (HFD) at Vostok compared with total solar irradiance (TSI) and volcanic aerosol forcing (VF). *TSI* indicates the reconstructed version of total solar irradiance (Wang et al. 2005). Heat flux density errors are calculated using the Monte-Carlo approach by varying of initial temperature within its standard deviation from its smoothed series with smoothing parameter a = 0.5. Vostok heat flux density (HFD) was calculated from observed temperatures and first value in 1958 was adjusted to annual energy balance which was measured at Dome A by Chen et al. (2010). Estimated volcanic forcing by Sato et al. (1993) is shown with gray line. Combined forcing TSI + 0.5VF is calculated assuming a linear combination which maximizes the correlation with HFD

estimated by the observer. Satellite based cloudiness estimations show a gap of cloudiness fraction over 75°–85° south latitude belt (e.g. Karlsson et al. 2013).

Total solar irradiance (TSI) flux was reconstructed by Wang et al. (2005) and updated with PMOD (Frohlich 2007) composite series. Data are available at http://lasp.colorado.edu/lisird/tss/historical_tsi.csv. Both modelling efforts for reconstruction TSI and composing of different satellite radiometers are difficult tasks. The difference between TSI composite series is debated up to day (see e.g. Scafetta and Willson 2009), but their difference is negligible for our target of indicating the amplitude and phase of 11-year TSI variation.

Global volcanic aerosol forcing series (VF) during the period of interest up to 2012 was estimated by Sato et al. (1993), Fig. 2. Effective VF by Sato et al. (1993) is calculated from the optical depth by scaling multiplier VF = −23τ, where optical depth τ is scaled in nm. It differs considerably from other versions, e.g. VF by Crowley (2000) is smoother and smaller. We use here Sato et al. (1993) version, because it is the only one which is continuously updated. Data are available at http://www.giss.nasa.gov/data/strataer/.

3 Inverse heat conductivity problem

Consider 1D heat transfer through an semi-infinite homogeneous space of ice heated on the boundary by heat flux $q(t)$. The problem is stated here as temperature conductivity equation:

$$\frac{\partial T}{\partial t} = \frac{\lambda}{\rho c}\frac{\partial^2 T}{\partial z^2} \tag{1}$$

Here λ and c = 1,741 J/kg/°K are specific heat conductivity and heat capacity of ice. Typical values of heat constants for ice are taken at −55 °C (Chen et al. 2010) and henceforth their temperature dependence is neglected for relatively small temperature range is considered (Fig. 3). Density grows with depth for first tenth of meters from 340 to 900 kg/m^3 (Chen et al. 2010) and influences considerably other heat constants. It is known that the density of the firn varies significantly down to depth of about 100 m, where dense ice forms. The density of the mixture can be approximated with the expression (Chen et al. 2010)

$$\rho = \rho_i - (\rho_i - \rho_s)\cdot\exp(-cz) \tag{2}$$

Here $\rho(z)$ is the density of snow mixture, constants ρ_i = 920 kg/m^3 and ρ_s = 340 kg/m^3 are densities of dense ice and surface snow. Heat conductivity varies with density as

$$\lambda = \lambda_a + (7.75\cdot 10^{-5}\rho + 1.11\cdot 10^{-6}\rho^2)\cdot(\lambda_i - \lambda_a) \tag{3}$$

Here λ_a = 0.024 W/(mK) is the conductivity of air, λ_i = 2.76 W/(mK) is conductivity of ice at temperature about −55 °C.

Time-dependent condition for active boundary is:

$$\lambda\frac{\partial T}{\partial z}_{Z=0} = q(t) \tag{4}$$

Flux on the passive boundary is assumed to be constant. Considering the active boundary flux as a periodical function

$$q = q_0\cos(\omega t), \tag{5}$$

the direct problem (1,4) has the analytical solution if λ and ρ assumed to be constants (Beck et al. 1985).

$$T(z,t) = T_0 + \frac{q_0}{\lambda}\sqrt{\frac{\alpha}{\omega}}\exp\left(-z\sqrt{\frac{\omega}{2\alpha}}\right)\cos\left(\omega t - z\sqrt{\frac{\omega}{2\alpha}} - \frac{\pi}{4}\right) \tag{6}$$

Here $\alpha = \frac{\lambda}{\rho c}$[m^2/s] is the temperature conductivity of ice. Characteristic depth $(2\alpha/\omega)^{1/2}$ for the decaying of the oscillation is under exponent. On the surface where z = 0 the solution is:

$$T(0,t) = T_0 + \frac{q_0}{\lambda}\sqrt{\frac{\alpha}{\omega}}\cos\left(\omega t - \frac{\pi}{4}\right) \tag{7}$$

We can see from Eq. 7 that harmonic oscillations of the HFD transform into harmonic temperature oscillations with

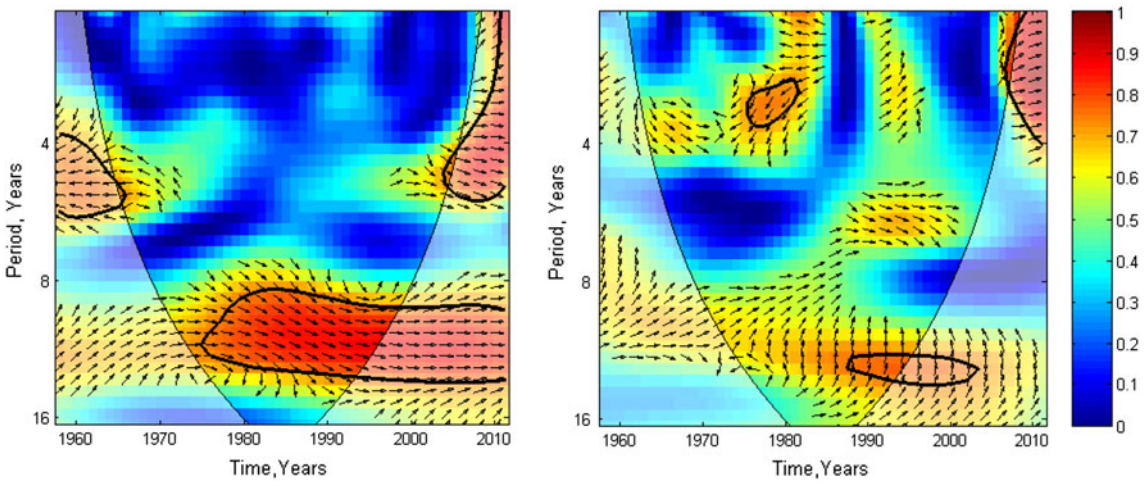

Fig. 3 Wavelet coherence between HFD and TSI (*left panel*) versus wavelet coherence between HFD and volcanic forcings (*right panel*). Thick contour shows the region of 95 % confidence against red noise. Level of the coherence is shown with *colour bar*. *Arrows* show the phase coherence (*right arrow*—signals are in phase, *left arrow*—in opposite phases). Confidence for wavelet coherence was estimated using Monte-Carlo method (Grinsted et al. 2004). The cone of influence where wavelet edge effects may disturb the results is shown as a *lighter shade*

the same period but with the phase shift (lag) 1/8 of period. The shape of the sunspot cycle is far from harmonic oscillation (see e.g. Volobuev 2006, 2009) and inverse problem should be solved.

Problem (1, 4) with known temperature on the surface and unknown HFD q(t) is called inverse heat conductivity problem (IHCP) (Beck et al. 1985). If λ and ρ are not constant (Eqs. 2, 3), the problem (1–4) becomes nonlinear. Direct problem has no analytical solution for this case. IHCP is ill-posed (Zhu et al. 2002) and solving requires the regularization procedure which leads to unavoidable difficulties with choosing the correct solution. The uniqueness for this solution can not be mathematically proved. That is why IHCP is solved for a number of climatic problems, e.g. for reconstruction of earth surface temperature from borehole data (Beltrami 2002) or for estimation of continental energy balance (Beltrami et al. 2002) with using an assumption that λ and ρ are constant.

We take some efficient values of the density at penetration depth of corresponding oscillation, for 11-year cycle the efficient density was chosen here $\rho = 473$ kg/m^3 which corresponds to 13 m effective depth of penetration this oscillation into ice. Efficient heat conductivity is calculated according to Eq. (3). This assumption allows us to remain within a frame of linear problem, which allows unique solution for inverse problem without iterations and growing of the instability. Choosing of this effective depth is not critical to results: setting $z = 50$ m, $\rho = 752$ kg/m^3 leads to the same phase oscillation of HFD with 20 % larger amplitude. Seasonal variation penetrates the ice down to 5–9 m (Chen et al. 2010) and penetration depth increases as the square root of oscillation period (Eq. 6) so expected depth for 11 year oscillation should be three times larger than that for the seasonal one.

The solution of IHCP is a digitized integral expression for HFD

$$q_i = 2\sqrt{\frac{\lambda\rho c}{\pi\Delta t}}\sum_{j=1}^{i}\left[T_{j-1} - T_j\right]\cdot\left[\sqrt{i-(j-1)} - \sqrt{i-j}\right] \tag{8}$$

Here Δt is 1 year time step 31536000 s, i is time step index and j is blind index. We use the difference $T_j - T_{j-1}$ calculated after spline approximation to provide the minimum error.

Results are shown in Fig. 2.

Heat flux density errors are calculated by varying of initial temperature within ±σ, where σ is standard deviation of temperature from its smoothed series (Fig. 1). All five HFD minima coincide with TSI minima within ±1 year. Epochs of maxima of TSI are more uncertain which is typical feature of solar indices. Correlation analysis between Vostok temperature-based data and two major forcings is shown in Table 1.

Heat flux density (Table 1, last column) has small but significant positive correlation with both TSI and VF indices whereas initial temperature series have insignificant correlation.

Smoothing effectively removes spikes from temperature series (Fig. 1) and makes correlation some higher (Table 1). The correlation remains insignificant if temperature is not recalculated into HFD according with Eq. 8. Choosing of smoothing parameter is possible in a wide range $0.1 < a < 1$ with significant correlations between forcings and HFD.

Although both forcings are almost equally important in sense of Pearson's correlation we can directly see from Fig. 2 that extremes are synchronized better for (HFD, TSI) pair than for (HFD, VF).

Table 1 Pearson's correlation between Vostok temperature-derived HFD data and forcings. *Error* shows 95 % confidence interval. Smoothing parameter a = 0.5

	Initial temperature	Smoothed temperature	HFD
Solar forcing (TSI)	0.06 ± 0.28	0.11 ± 0.28	0.50 ± 0.24
Volcanic forcing (VF)	−0.16 ± 0.27	0.09 ± 0.28	0.41 ± 0.25

We can quantify this fact with wavelet coherence (Grinsted et al. 2004) analysis for both pairs (Fig. 3). Wavelet coherence is often interpreted as a localized correlation coefficient in time frequency space. Wavelet coherence for (HFD, TSI) pair is definitely stronger than for (HFD, VF) pair (Fig. 3, Left and Right panels respectively), because 95 % confidence contour covers more than 75 % of (11 ± 1) years period band for (HFD, TSI) but smaller than 25 % coverage (HFD, VF) excepting wavelet cone-of-influence regions. Moreover, high wavelet coherence for (HFD, TSI) pair is confirmed with phase coherence as shown by arrows directed mostly to the right in Left panel of Fig. 3 whereas it is not confirmed for (HFD, VF) pair where arrows are mostly directed upside showing a considerable phase shift even for relatively small domain of 95 % confident wavelet coherence. These both forcings should have an impact on the HFD but the model beyond volcanic aerosol forcing may be not fully developed at the moment, because of considerable difference between available series [e.g. by Crowley (2000) and Sato et al. (1993)].

Assuming the linear empirical model from available data, F = TSI + k × VF and adjusting k we found a maximum of Pearson's correlation r = 0.63 ± 0.22 between F and HFD with k = 0.5. This combined forcing is also presented in Fig. 2. Believing this small k the amplitude of VF by Sato et al. (1993) is probably overestimated.

4 Discussion

It is known that polar regions are heat sinks, i.e. they emit more heat (infrared radiation) into space than they absorb (short wave radiation) (Trenberth and Caron 2001). The balance is sustained with meridional heat transfer via mixing of the atmosphere and ocean. Heat coming to Antarctica from lower latitudes is absorbed into ice with turbulent flux from air (Chen et al. 2010). Vertical heat flux near the surface of ice is originated from the latitude-dependent energy balance. Following to the model of Gal-Chen and Schneider (1975), we can present this balance as

$$R\frac{\partial T}{\partial t} = (1-A)Q_S + V - F_{IR} + \frac{1}{\sin\vartheta}\frac{\partial}{\partial y}\sin\vartheta\left(F_0 + F_A + F_q\right) \equiv q(t) \quad (9)$$

here first two terms are solar and VFs, F_{IR} is outgoing infrared radiation. F_0, F_A, and F_q are zonal heat fluxes of ocean circulation, atmosphere mixing and the transport of latent heat respectively. ϑ is colatitude and $y = a\vartheta$, a is radius of the Earth. Albedo A depends on latitude and temperature. It forms the positive feedback due to extending of ice fields with decreasing of temperature. Fluxes F_0, F_A, and F_q depend on the latitudianal temperature gradient and the average meridian wind velocity. R is the thermal inertia. It is not easy task to estimate all fluxes in Eq. (9), different parameterizations lead to different results (Gal-Chen and Schneider 1975). The balancing flux $q(t)$ depends not only on solar and VFs but also it depends on the temperature and its latitudianal gradient through IR and meridian fluxes. Probably this is the main reason for different trends in forcings series and HFD shown in Fig. 2 and for relatively small correlations presented in Table 1. It may be possible for future work to arrange available global data and apply minimum assumptions to calculate four non-stationary fluxes F_{IR}, F_0, F_A, and F_q in Eq. (9) and extract clearer temperature-based response function

$$\Psi \equiv q(t) + F_{IR} - \frac{1}{\sin\vartheta}\frac{\partial}{\partial y}\sin\vartheta\left(F_0 + F_A + F_q\right) \quad (10)$$

which should present more direct response of the climate to forcings. Direct comparison in Fig. 2 is possible with strong assumption of the balance between last two terms in Eq. 10, i.e. outgoing IR flux is compensated by meridianal heat transfer. This assumption may be not perfectly completed, which may be one of the reasons for low correlations in Table 1. Other reasons are small but non-zero local climate disturbances (Fig. 1). On the other hand meridianal heat flux intensity should also depend on the insolation from basic physical consideration of the spherical planet (Stone 1978) and some extended model needs to be developed in future to take into account all possible dependences.

Considering constrains shown by data, it is interesting that 11-year variation can be directly seen in smoothed temperature data with amplitude 0.5–1 °C, (Fig. 1) which is higher than global average estimation (0.1 °C per 0.1 % of insolation change, see e.g. Budyko 1968), but very close to 0.3–0.8 °C per 0.1 % estimations by Gal-Chen and Schneider (1975) for the south 80° latitude belt.

Wide uncertainty of temperature response in the model is defined by the uncertainty of the albedo and fluxes F_O, F_A, F_q parameterization.

5 Conclusions

Unique climatic conditions of Central Antarctica provide the great possibilities to study the climate response mechanisms on the global forcings. Ending this pilot study we can conclude that

- HFD variations in Central Antarctic show significant correlation with both solar cycle ($r = 0.50 \pm 0.24$) and VF ($r = 0.41 \pm 0.25$). Wavelet coherence is stronger and shows better phase agreement for HFD and TSI.
- Linear combination of forcings TSI + 0.5VF maximizes the correlation to $r = 0.63 \pm 0.22$, so the amplitude of VF by Sato et al. (1993) is likely overestimated.
- HFD variations are in-phase with solar cycle so that all five (100 %) of observed HFD minima coincides with minima of TSI within ±1 year.
- Smoothed temperature amplitude response on TSI variation from minimum to maximum of solar cycle is close to the predictions of the model by Gal-Chen and Schneider (1975) describing the polar amplification effect, so 11-year variation of HFD that we see near the polar cap is likely a global effect caused by polar amplification feedback rather than just a response to local variations of the insolation and VFs.

Acknowledgments I am indebted to both anonymous Referees for thoughtful reading of the manuscript and useful suggestions. I thank AARI and RAE teams for making meteorological data for Vostok available online, as well I thank cited Authors of TSI and VFs reconstructions. Wavelet coherence software http://noc.ac.uk/using-science/crosswavelet-wavelet-coherence was provided by A. Grinsted. Special thank to my colleagues from 43rd RAE winter at Vostok. The work was supported by grants: Program of Presidium of Russian Academy of Science N 22, Russian Foundation for Basic Research N 10-02-00391-a, 11-02-00755-a and Scientific School-1625.2012.2.

References

Beck JV, St Clair CR, Blackwell B (1985) Inverse heat conduction. Wiley, New York

Beltrami H (2002) Climate from borehole data: energy fluxes and temperatures since 1500. Geophys Res Lett 29(23):2111

Beltrami H, Smerdon JE, Pollack HN, Huang S (2002) Continental heat gain in the global climate system. Geophys Res Lett 29(8):1167

Budyko MI (1968) The effect of solar radiation variations on the climate of the Earth. Tellus 21:611–619

Chen B, Zhang R, Sun S, Bian L, Xiao C, Zhang T (2010) A one-dimensional heat transfer model of the Antarctic Ice Sheet and modeling of snow temperatures at Dome A, the summit of Antarctic Plateau. Sci China Earth Sci 53(5):763–772

Crowley TJ (2000) Causes of climate change over the past 1000 years. Science 289:270–277

Eichler A, Olivier S, Henderson K, Laube A, Beer J, Papina T, Gäggeler HW, Schwikowski M (2009) Temperature response in the Altai region lags solar forcing. Geophys Res Lett 36:L01808. doi:10.1029/2008GL035930

Foukal P, Fröhlich C, Spruit H, Wigley TML (2006) Variations in solar luminosity and their effect on the Earth's climate. Nature 443:161–166

Frohlich C (2007) Solar irradiance variability since 1978. Solar Variability and Planetary Climates, 53–65

Frolich C, Lean J (1998) The Sun's total irradiance: cycles, trends and related climate change uncertainties since 1976. Geophys Res Lett 25:4377

Gal-Chen T, Schneider SH (1975) Energy balance climate modeling: comparison of radiative and dynamic feedback mechanisms. Tellus 28:108–121

Gregory JM, Forster PM (2008) Transient climate response estimated from radiative forcing and observed temperature change. J Geophys Res, 113(D23)

Gregory JM, Ingram WJ, Palmer MA, Jones GS, Stott PA, Thorpe RB, Lowe JA, Johns TC, Williams KD (2004) A new method for diagnosing radiative forcing and climate sensitivity. Geophys Res Lett 31:L03205. doi:10.1029/2003GL018747

Grinsted A, Moore JC, Jevrejeva S (2004) Application of the cross wavelet transform and wavelet coherence to geophysical time series. Nonlinear Process Geophys 11(5/6):561–566

Karlsson KG, Riihelä A, Müller R, Meirink JF, Sedlar J, Stengel M, Wolters E (2013) CLARA-A1: a cloud, albedo, and radiation dataset from 28 yr of global AVHRR data. Atmos Chem Phys 13(10):5351–5367

Kiehl JT (2007) Twentieth century climate model response and climate sensitivity. Geophys Res Lett 34:L22710. doi:10.1029/2007GL031383

Knutti R, Krahenmann S, Frame DJ, Allen MR (2008) Comment on "Heat capacity, time constant, and sensitivity of Earth's climate system" by S. E. Schwartz. J Geophys Res 113:D15103. doi:10.1029/2007JD009473

Langen PL, Alexeev VA (2007) Polar amplification as a preferred response in an idealized aquaplanet GCM. Clim Dyn 29:305–317. doi:10.1007/s00382-006-0221-x

Lean J, Beer J, Bradley R (1995) Reconstruction of solar irradiance since 1610: implications for climate change. Geophys Res Lett 22(23):3195–3198

Sato M, Hansen JE, McCormick MP, Pollack JB (1993) Stratospheric aerosol optical depth, 1850–1990. J Geophys Res 98:22987–22994

Scafetta N, West BJ (2007) Phenomenological reconstructions of the solar signature in the Northern Hemisphere surface temperature records since 1600. J Geophys Res 112(D24):D24S03

Scafetta N, Willson RC (2009) ACRIM-gap and TSI trend issue resolved using a surface magnetic flux TSI proxy model. Geophys Res Lett 36:L05701. doi:10.1029/2008GL036307

Schneider EK, Kirtman BP, Lindzen RS (1999) Tropospheric water vapor and climate sensitivity. J Atmos Sci 56:1649–1658

Schwartz SE (2007) Heat capacity, time constant, and sensitivity of Earth's climate system. J Geophys Res 112:D24S05. doi:10.1029/2007JD008746

Sirocko F, Brunck H, Pfahl S (2012) Solar influence on winter severity in central Europe. Geophys Res Lett 39(16):L16704

Solanki SK, Fligge M (1999) A reconstruction of total solar irradiance since 1700. Geophys Res Lett 26(16):2465–2468

Stevens MJ, North GR (1996) Detection of the climate response to the solar cycle. J Atmos Sci 53:2594–2608

Stone PH (1978) Constraints on dynamical transports of energy on a spherical planet. Dyn Atmos Oceans 2(2):123–139

Trenberth KE, Caron JM (2001) Estimates of meridional atmosphere and ocean heat transports. J Clim 14(16):3433–3443

Volobuev D (2006) "TOY" dynamo to describe the long-term solar activity cycles. Sol Phys 238(2):421–430

Volobuev DM (2009) The shape of the sunspot cycle: a one-parameter fit. Sol Phys 258(2):319–330

Wang YM, Lean JL, Sheeley NR Jr (2005) Modeling the Sun's magnetic field and irradiance since 1713. Astrophys J 625(1):522

Wilson RC, Mordvinor AV (2003) Secular total solar irradiance trend during solar cycles 21–23. Geophys Res Lett 30:1199

Zhou J, Tung KK (2010) Solar cycles in 150 years of global sea surface temperature data. J Clim 23(12):3234–3248

Zhu J, Kamachi M, Wang D (2002) Estimation of air-sea heat flux from ocean measurements: an ill-posed problem. J Geophys Res 107(C10):3159